# Terahertz-Raman Spectroscopy of Ligand-Protected $Au_8$ Clusters

*Masaru Kato,*[*†,‡] *Yukatsu Shichibu,*[†,‡] *Kazuya Ogura,*[‡] *Mitsuhiro Iwasaki,*[‡] *Mizuho Sugiuchi,*[‡] *Katsuaki Konishi,*[†,‡] *and Ichizo Yagi*[*,†,‡]

[†]Faculty of Environmental Earth Science and [‡]Graduate School of Environmental Science, Hokkaido University, N10W5, Kita-ku, Sapporo 060-0810, Japan.

AUTHOR INFORMATION

**Corresponding Author**

*masaru.kato@ees.hokudai.ac.jp (to MK) *iyagi@ees.hokudai.ac.jp (to IY)

ABSTRACT. For ligand-protected gold clusters, geometrical differences of gold cores and/or the presence of secondary gold core–ligand interactions influence their unique optical and electronic properties and can, in principle, be detected by spectral changes of gold core vibrations (phonon modes) in ultra-low-frequency Raman spectroscopy. We report experimental and theoretical Raman spectra of $Au_8$ clusters protected by phosphine ligands particularly in the "gold cluster fingerprint" region from 50 to 150 $cm^{-1}$ Raman shift (1.5 to 4.5 terahertz). A characteristic core breathing mode observed at ca. 123 $cm^{-1}$ was sensitive to differences of core geometries. A new band was found at ca. 150 $cm^{-1}$ originating from a local strain on a polyhedral gold core caused by weak Au···π interactions. THz Raman spectroscopy would be utilized for metal nanoclusters to visualize core structural changes and Au···π interactions, which cannot be captured by single crystal X-ray analysis.

**TOC GRAPHICS**

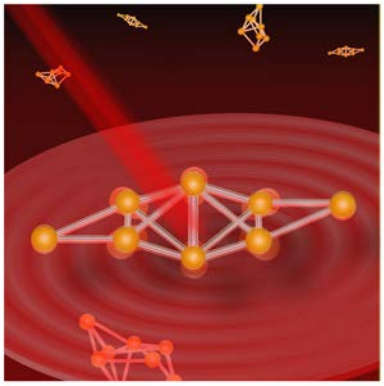

Atomically precise gold clusters have unique optical and electronic properties,[1-2] and have potential applications such as light energy conversion,[3] catalysis[4-6] and biosensing,[7] compared with their larger counterparts that show localized surface plasmon resonance. These clusters are stabilized and isolated with organic ligands such as thiolates and phosphines.[2,8-9] The coordination of mono- and bidentate ligands dictates the number of gold atoms and the morphology of the polyhedral gold core unit for ligand-protected gold clusters.[8,10] Their unique optical and electronic properties often originate from their gold frameworks,[11] which can be determined by the single crystal X-ray diffraction. These properties are also known to be quite sensitive to secondary core–ligand interactions such as Au···π interactions.[12-14] Such weak interactions can cause local strain of the gold core unit, which can be visualized by vibrational and nuclear resonance spectroscopic techniques,[13-14] rather than the single crystal X-ray analysis. These spectroscopic techniques enable us to extract direct information on secondary core–ligand interactions from ligands but not from the gold core unit.

Ultra-low-frequency Raman spectroscopy at < 200 $cm^{-1}$ Raman shift (< ca. 6 terahertz (THz)), called THz Raman spectroscopy, can, in principle, give us the direct experimental information of ligand-protected gold clusters on not only core geometrical changes but also the local strain of the core unit caused by core–ligand interactions.[15-16] Raman spectroscopy is a powerful technique to observe phonon modes, which are sensitive to the local strain of nanomaterials such as graphene.[17-19] Typical Raman spectra recorded in the range from 200 to 4000 $cm^{-1}$ provide vibrational information on covalent and coordination bonds but not on the gold core unit of gold clusters. To investigate gold cluster vibrations, Raman spectra in the ultra-low frequency region need to be obtained. Theoretical[20-23] and experimental studies including femtosecond transient absorption spectroscopy[11,24-26] suggest that phonon modes of gold clusters (vibrations of the gold

core unit) can be observed in the THz region. In the traditional approach, THz Raman spectra are collected using a multiple monochromator, which often suffers from low signal intensity and long integration time.[27-29] In contrast, modern Raman microscopes equipped with a single monochromator and a notch filter give high signal intensity. However, such modern Raman microscopes usually are not accessible to the THz region because of the difficulty in elimination of Rayleigh scattering from the excitation laser,[30-32] which makes vibrational studies on phonon modes of gold clusters challenging.[15]

Herein, we report experimental and theoretical studies on THz Raman spectroscopy of atomically precise gold clusters protected by phosphine ligands. We used a Raman microscope system equipped with an amplified spontaneous emission suppression filter and two ultra-narrow-band Notch filters to obtain Raman spectra in the ultra-low-frequency region. We selected $Au_8$ clusters with a bidentate ligand of 1,3-bis(diphenylphosphino)propane (dppp) and a terminal ligand (X) or a monodentate ligand of triphenylphosphine ($PPh_3$): $[Au_8X_2(dppp)_4]^{2+}$ and $[Au_8(PPh_3)_8]^{2+}$ salts. The $Au_8$ clusters of $[Au_8X_2(dppp)_4]^{2+}$ and $[Au_8(PPh_3)_8]^{2+}$ have different gold frameworks: the former has a [core + *exo*]-type $Au_8$ framework (**Figure 1a**)[13,33] whereas the latter has a capped centered chair framework (**Figure 1b**).[34-35] Particularly for $[Au_8X_2(dppp)_4]^{2+}$, various monodentate ligands can be used as the terminal ligand X, keeping the same framework but changing the presence/absence of core–ligand interactions,[12-13,33] providing an ideal platform to investigate structural differences of gold frameworks and weak secondary core–ligand interactions in THz Raman spectroscopy.

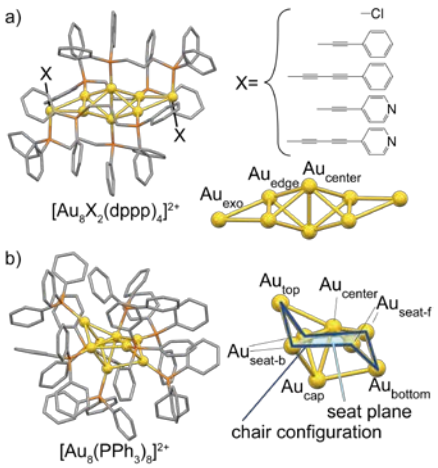


**Figure 1.** Structures of (a) $[Au_8X_2(dppp)_4]^{2+}$ (X = Cl, $C_2Ph$, $C_4Ph$, $C_2py$, $C_4py$)[33] and (b) $[Au_8(PPh_3)_8]^{2+}$.[34]

Firstly, THz Raman spectra of $[Au_8Cl_2(dppp)_4](PF_6)_2$ (**1**) and $[Au_8(PPh_3)_8](NO_3)_2$ (**2**)[33-35] were collected (**Figures 2a and 2b**). These Raman spectra revealed that the spectral feature at <200 $cm^{-1}$ Raman shift (<6 THz) highly depends on the $Au_8$ framework. Three broad bands were observed at ca. 20, 60 and 120 $cm^{-1}$ Raman shift for **1** whereas two broad bands were found at ca. 20 and 80 $cm^{-1}$ for **2**, where there is no band at ca. 120 $cm^{-1}$ (**Figures 2a and 2b**). These Raman bands are associated with vibrations of gold frameworks.[15,23] Particularly, the characteristic band at 120 $cm^{-1}$ for **1** originates from a vibrational mode of the [core + *exo*]-type geometry.

To understand band positions of gold cluster vibrations in detail, we performed peak deconvolution analysis of the obtained THz Raman spectra. The analysis required at least seven peaks to reproduce the experimental spectra of **1** and **2** (**Figures 2a and 2b**). All peak positions and relative intensities obtained in the peak deconvolution analysis are summarized in **Table 1**. The characteristic band at ca. 120 $cm^{-1}$ for **1** was fitted with a deconvoluted peak at 123.3 $cm^{-1}$.

The most intense broad peak at ca. 20 $cm^{-1}$ was deconvoluted into two peaks at 14.1 and 24.4 $cm^{-1}$ for **1** and 9.9 and 25.5 $cm^{-1}$ for **2**. The analysis also gave deconvoluted peaks at 61.8 $cm^{-1}$ for **1** and 84.2 $cm^{-1}$ for **2**.

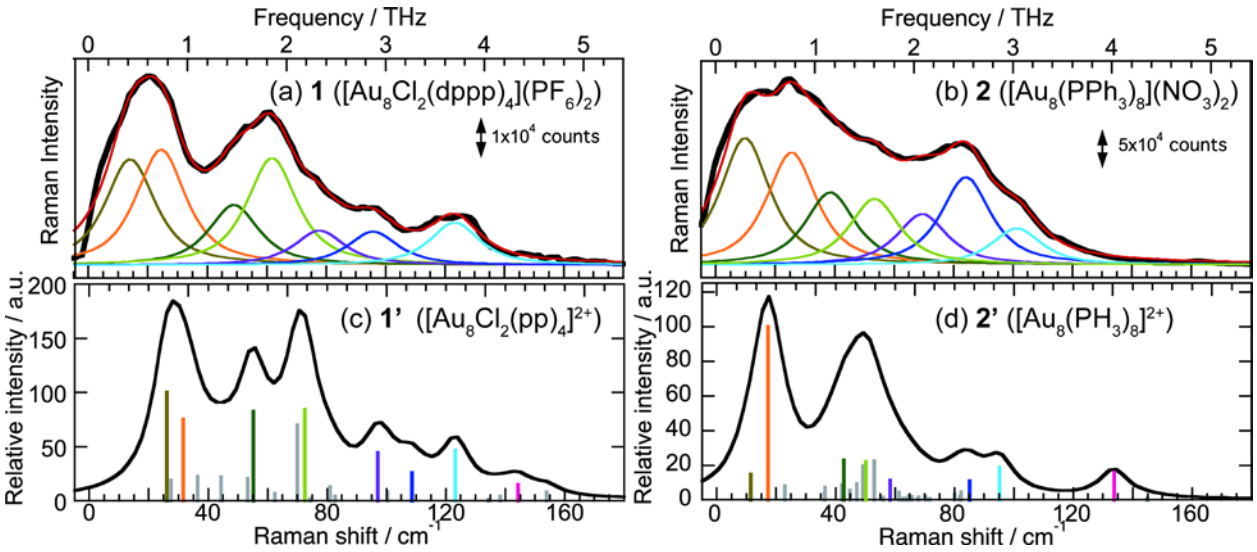


**Figure 2**. Experimental THz Raman spectra (the traces in black) of (a) **1** ($[Au_8Cl_2(dppp)_4](PF_6)_2$) and (b) **2** ($[Au_8(PPh_3)_8](NO_3)_2$) with seven deconvoluted peaks. Excitation wavelength: 785 nm; power input: ~1 mW. Simulated Raman spectra of model clusters of (c) **1'** ($[Au_8Cl_2(pp)_4]^{2+}$) and (d) **2'** ($[Au_8(PH_3)_8]^{2+}$). Calculated relative Raman intensities are also represented as colored sticks.

**Table 1.** Raman shifts ($cm^{-1}$) of deconvoluted peaks of clusters **1** and **2** and DFT simulated peaks of **1'** and **2'**. All simulated peaks are available in Tables S1 and S2. Movies showing these vibrational modes are available in the SI.

| **Raman shift / $cm^{-1}$ (Relative intensity / %)** | | **Mode description** [a] |
|---|---|---|
| **1** | **1'** | |
| 14.1 (92) | 26.13 (100) | $\delta(Au_{exo}–Au_{edge}–Au_{center})$ & $\nu(Au_{edge}–Au_{exo})$ |
| 24.4 (100) | 31.60 (75) | $\nu_{lib}(Au_{edge}–Au_{exo})$, $\nu_{lib}(Au–P)$[b] & $\nu_{lib}(Au–Cl)$ |
| 49.0 (52) | 55.21 (83) | $\nu_s(Au_{edge}–Au_{center}–Au_{edge})$ & $\nu_s(Au_{edge}–Au_{exo}–Au_{edge})$ |
| 61.8 (93) | 72.52 (84) | $\nu_{as}(Au_{edge}–Au_{center}–Au_{edge})$ |
| 77.8 (30) | 97.09 (44) | $\nu(Au_{center} – Au_{center})$, $\nu_{lib}(Au–P)$[b] & $\nu_{lib}(Au–Cl)$ |
| 95.8 (29) | 108.59 (26) | $\nu(Au_{center}–Au_{center})$, $\nu_{lib}(Au–P)$[b] & $\nu_{lib}(Au–Cl)$ |
| 123.3 (37) | 123.23 (47) | $Au_6$ core breathing |
| - | 144.23 (15) | $\nu(Au_{edge}– Au_{edge})$ |
| **2** | **2'** | |
| 9.9 (100) | 11.37 (15) | $\delta(Au_{seat\text{-}b}–Au_{center}–Au_{seat\text{-}f})$[c] |
| 25.5 (89) | 17.33 (100) | $\delta(Au_{seat\text{-}f}–Au_{center}–Au_{seat\text{-}f})$ |
| 38.5 (57) | 42.70 (23) | $\nu(Au_{seat\text{-}b}–Au_{seat\text{-}f})$ |
| 53.4 (52) | 50.20 (22) | $\delta(Au_{seat\text{-}b}–Au_{center}–Au_{seat\text{-}f})$ |
| 69.4 (40) | 58.33 (11) | $\nu_{lib}(Au–P)$ |
| 84.2 (69) | 85.16 (11) | $\nu_{as}(Au_{seat\text{-}b}–Au_{center}–Au_{seat\text{-}f})$ |
| 101.3 (29) | 95.19 (19) | Seat expanding |

a) $\nu$, $\delta$, $\nu_s$, $\nu_{as}$ and $\nu_{lib}$ indicate stretching, bending, symmetric stretching, asymmetric stretching and libration modes, respectively. b) These Au–P libration modes involve the pp ligands that are coordinated to the $Au_{center}$ and $Au_{exo}$ atoms. c) Diagonal $Au_{seat\text{-}b}–Au_{center}–Au_{seat\text{-}f}$.

To assign bands experimentally obtained in the THz region and understand why **1** showed the characteristic band at 123.3 $cm^{-1}$, density functional theory (DFT) calculations of model $Au_8$ clusters. For **1** and **2**, model $Au_8$ clusters of $[Au_8Cl_2(pp)_4]^{2+}$ (**1'**, pp = 1,3-bis(phosphino)propane) and $[Au_8(PH_3)_8]^{2+}$ (**2'**) were selected, respectively (See more details in the Supporting Information, SI). DFT calculations of **1'** produced a simulated Raman spectrum and showed a peak at 123.23 $cm^{-1}$, which mainly involves a $Au_6$ core breathing with a $Au_{center}$–$Au_{center}$ stretching (**Figure 3a**). Based on this peak, the deconvoluted Raman band at 123.3 $cm^{-1}$ for **1** can be assigned to a breathing mode of the octahedral $Au_6$ core unit. Similar core breathing modes were reported for theoretical calculations of $[Au_{38}(SH)_{24}]$ and $[Au_{37}Cl_2(SCH_3)_{10}(PPh_3)_{10}]^+$ clusters at ca. 105 $cm^{-1}$.[21-22] The corresponding band at 101.3 $cm^{-1}$ for **2** can be assigned to the peak at 95.19 $cm^{-1}$ mainly involving $Au_{seat\text{-}b}$–$Au_{seat\text{-}f}$ stretching, which looks like a seat expanding for **2'** (**Figure 3b**). This mode is obviously different from the core breathing mode of **1'**. Therefore, the $Au_6$ core breathing mode of **1** at 123.3 $cm^{-1}$ is characteristic.

The two deconvoluted peaks at ca. 20 $cm^{-1}$ found for **1** and **2** could be associated with bending, stretching and libration modes involving three gold atoms. The bands at 14.1 and 24.4 $cm^{-1}$ for **1** correspond to those at 26.13 and 31.60 $cm^{-1}$ for **1'**, respectively. The former peak is the highest for **1'** and can be assigned to $Au_{exo}$–$Au_{edge}$–$Au_{center}$ bending modes ($\delta(Au_{exo}–Au_{edge}–Au_{center})$) coupled with the stretching of the $Au_{edge}$–$Au_{exo}$ bonds ($\nu(Au_{edge}–Au_{exo})$), as shown in **Figure 3a**. The deconvoluted peaks at 9.9 and 25.5 $cm^{-1}$ for **2** correspond to those at 11.37 and 17.33 $cm^{-1}$ for **2'**, respectively. The latter peak is the highest and is associated with a bending mode of $Au_{seat\text{-}f}$–$Au_{center}$–$Au_{seat\text{-}f}$ ($\delta(Au_{seat\text{-}f}–Au_{center}–Au_{seat\text{-}f})$, **Figure 3b**). Although $Au_8$ frameworks are different between the clusters **1** and **2**, these band positions are quite close each other, implying

that phonon bands at ca. 20 $cm^{-1}$ are not quite sensitive to the framework of gold clusters. Actually, phonon bands at ca. 20 $cm^{-1}$ were reported for other ligand-protected gold clusters even with different gold frameworks and the number of gold atoms in femtosecond transient absorption spectroscopy.[11,24-25]

In contrast, the deconvoluted peaks at 61.8 $cm^{-1}$ for **1** and 84.2 $cm^{-1}$ for **2** were sensitive to the $Au_8$ framework. The band at 61.8 $cm^{-1}$ corresponds to the band at 72.52 $cm^{-1}$ with the asymmetric stretching of $Au_{edge}–Au_{center}–Au_{edge}$ ($\nu_{as}(Au_{edge}–Au_{center}–Au_{edge})$) for **1'** (**Figures 3a**). The band at 84.2 $cm^{-1}$ can be assigned to $\nu_{as}(Au_{seat\text{-}b}–Au_{center}–Au_{seat\text{-}f})$ at 85.16 $cm^{-1}$ for **2'** (**Figures 3b**). Although these bands are similar asymmetric stretching modes, there is a peak shift by ca. 20 $cm^{-1}$. It seems that the Raman band positions of these asymmetric stretching modes are influenced by differences of $Au_8$ frameworks, like the core breathing mode. This finding suggests that the ultra-low vibrational region particularly from 50 to 150 $cm^{-1}$ Raman shift (1.5 to 4.5 THz) would be used as the "fingerprint" region for ligand-protected gold clusters.[11,20-25]

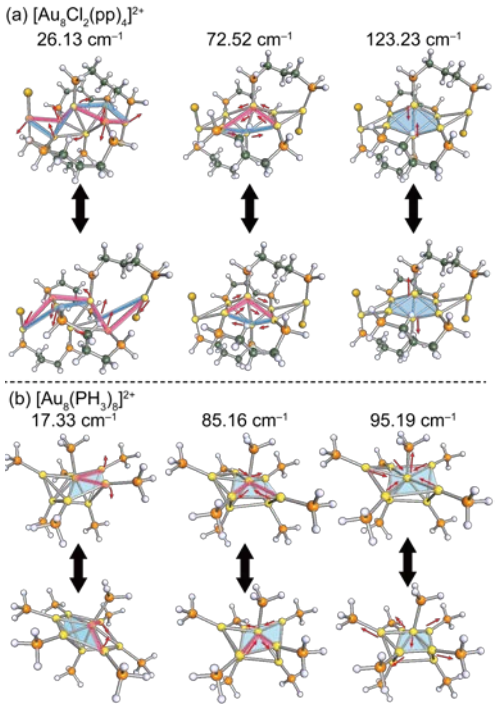


**Figure 3**. (a) Representative vibrational modes of **1'** at 26.13 $cm^{-1}$ for $\delta(Au_{exo}–Au_{edge}–Au_{center})$ and $\nu(Au_{edge}–Au_{exo})$, 72.52 $cm^{-1}$ for $\nu_{as}(Au_{edge}–Au_{center}–Au_{edge})$, and 123.23 $cm^{-1}$ for the $Au_6$ core breathing. (b) Representative vibrational modes of **2'** at 17.33 $cm^{-1}$ for $\delta(Au_{seat\text{-}f}–Au_{center}–Au_{seat\text{-}f})$, 85.16 $cm^{-1}$ with $\nu_{as}(Au_{seat\text{-}b}–Au_{center}–Au_{seat\text{-}f})$ and 95.19 $cm^{-1}$ for the seat expanding mode. Seat planes are also shown in blue for **2'**. Au, P, C, H and Cl atoms are in yellow, orange, green, white and brown, respectively. Movies showing these vibrational modes are available in the SI.

Next, we collected THz Raman spectra of $Au_8$ clusters with mono- and di-acetylenic ligands, $[Au_8X_2(dppp)_4](NO_3)_2$, where X = C≡C–Ph ($C_2Ph$), C≡C–4-py ($C_2py$), C≡C–C≡C–Ph ($C_4Ph$) or C≡C–C≡C–4-py ($C_4py$) to investigate secondary core–ligand interactions using THz Raman spectroscopy. Interestingly, a characteristic band was observed at ca. 150 $cm^{-1}$ for the di-

acetylenic $Au_8$ clusters but not for the mono-acetylenic ones in the THz Raman spectra (**Figure 4a**). The peak deconvolution analysis of the THz Raman spectra required at least seven peaks for the mono-acetylenic clusters but eight peaks for the di-acetylenic ones. The eighth peak was found at 143.5 $cm^{-1}$ for the $C_4$Ph cluster and 149.9 $cm^{-1}$ for the $C_4$py cluster (**Table S3**). This characteristic band can be assigned to a stretching mode of $Au_{edge}$–$Au_{edge}$ bonds ($\nu(Au_{edge}–Au_{edge})$) at 144.23 $cm^{-1}$ in the simulated spectra of **1'** (**Table 1** and the SI). Since there is the attractive Au···π interaction between the coordinating carbon atom ($C_\alpha$) and the $Au_{edge}$ atom for the di-acetylenic clusters but not for the mono-acetylenic ones (**Figure 4b**),[13] it is most likely that the local strain on the $Au_{edge}$–$Au_{edge}$ bond in the $Au_6$ core unit is caused by the Au···π interaction, leading to the emergence of the characteristic peak. Notably, the relative peak intensity of the $C_4$py cluster was higher than that of the $C_4$Ph (**Table S3**), indicating that the Au···π interaction for $C_4$py could be stronger than that for $C_4$Ph.

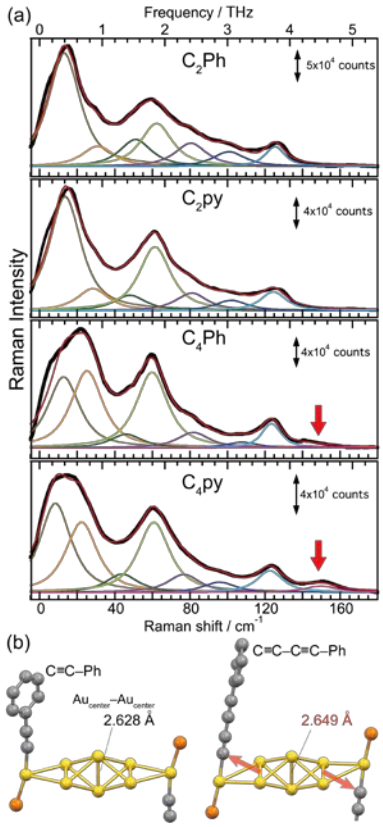


**Figure 4.** (a) THz Raman spectra of mono- and di-acetylenic $Au_8$ clusters of $[Au_8X_2(dppp)_4](NO_3)_2$ (X = $C_2Ph$, $C_2py$, $C_4Ph$, $C_4py$) with deconvoluted peaks. Excitation wavelength: 785 nm; power input: ~1 mW. Arrows in red indicate the characteristic peak for the di-acetylenic $Au_8$ clusters. (b) Schematic representation of the $Au_8$ framework of the $C_2Ph$ and $C_4Ph$ complexes with $Au_{center}$–$Au_{center}$ bond lengths.[13,36]. The red arrows indicate Au···π interactions between the $C_\alpha$ atom of $C_4Ph$ and the $Au_{edge}$ atom.

We also observed lower frequency peak shifts of the $Au_6$ core breathing mode for the di-acetylenic clusters by ca. –2 $cm^{-1}$, relative to the corresponding mono-acetylenic clusters: 125.4 $cm^{-1}$ for $C_2Ph$; 124.5 $cm^{-1}$ for $C_2py$; 123.5 $cm^{-1}$ for $C_4Ph$; 122.6 $cm^{-1}$ for $C_4py$ (**Table S3**). In general, the vibrational frequency decreases as the chemical bond length increases. Conversely,

as chemical bond lengths are shortened, relative to their normal lengths, Raman peak positions shifted to higher frequencies.[17-19] The $Au_{center}$–$Au_{center}$ bond for the $C_4Ph$ cluster (2.649 Å) is longer than that for the $C_2Ph$ cluster (2.628 Å) (**Figure 4b**).[13,36] Furthermore, the $Au_6$ core breathing mode mainly involves the $Au_{center}$–$Au_{center}$ stretching (**Figure 3a**). Thus, the lower frequency shift of the $Au_6$ core breathing mode was observed for the di-acetylenic clusters. Our findings suggest that THz Raman spectroscopy would be used to visualize local strain of gold cores caused by weak Au···π interactions.

In conclusion, we investigated experimental and theoretical Raman spectra of phosphine-protected $Au_8$ clusters particularly in the fingerprint region from 50 to 150 $cm^{-1}$ Raman shift (1.5 to 4.5 THz). The $Au_6$ gold core breathing mode was observed at ca. 123 $cm^{-1}$ for **1** that has the [core + *exo*]-type $Au_8$ framework. This characteristic peak allowed us to distinguish **1** from **2** that has the different capped centered $Au_8$ framework. For di-acetylenic $Au_8$ clusters with the [core + *exo*]-type framework, even weak Au···π interactions between the $C_\alpha$ atom of di-acetylenic ligands and the $Au_{edge}$ atom caused the local strain on the $Au_6$ gold core, leading to the appearance of the characteristic band at ca. 150 $cm^{-1}$. Our findings demonstrate that THz Raman spectroscopy would provide the direct experimental information on phonon modes and the local core strain for ligand-protected metal clusters, which cannot be visualized by the single crystal X-ray analysis. THz Raman spectroscopy would become a powerful technique to characterize metal clusters with different metal frameworks and secondary core–ligand interactions, which would encourage us to design and synthesize new metal clusters with unique phonon-coupled optical properties.

ASSOCIATED CONTENT

**Supporting Information**.

The following files are available free of charge.

Experimental section and Raman shifts of simulated and deconvoluted peaks (PDF)

Movies showing vibrational modes of **1'** and **2'** (mp4)

AUTHOR INFORMATION

**Notes**

The authors declare no competing financial interests.

ACKNOWLEDGMENTS

The authors thank Shingo Mukai and Yusuke Kawamura (Technical Division, Institute for Catalysis, Hokkaido University) for their technical support on THz Raman setups. This work was supported by Grant-in-Aid for Young Scientists (B) (No. 16K20882 to MK), and Scientific Research (B) (No. 19H02664 to IY) and a MEXT Program for Development of Environmental Technology using Nanotechnology from the Ministry of Education, Culture, Sports, Science and Technology, Japan.

REFERENCES

(1) Kang, X.; Zhu, M. Tailoring the photoluminescence of atomically precise nanoclusters. *Chem. Soc. Rev.* **2019,** *48*, 2422-2457, DOI: 10.1039/C8CS00800K.

(2) Konishi, K.; Iwasaki, M.; Shichibu, Y. Phosphine-Ligated Gold Clusters with Core+exo Geometries: Unique Properties and Interactions at the Ligand–Cluster Interface. *Acc. Chem. Res.* **2018,** *51*, 3125-3133, DOI: 10.1021/acs.accounts.8b00477.

(3) Abbas, M. A.; Kamat, P. V.; Bang, J. H. Thiolated Gold Nanoclusters for Light Energy Conversion. *ACS Energy Lett.* **2018,** *3*, 840-854, DOI: 10.1021/acsenergylett.8b00070.

(4) Higaki, T.; Li, Y.; Zhao, S.; Li, Q.; Li, S.; Du, X.-S.; Yang, S.; Chai, J.; Jin, R. Atomically Tailored Gold Nanoclusters for Catalytic Application. *Angew. Chem. Int. Ed.* **2019,** *58*, 8291-8302, DOI: 10.1002/anie.201814156.

(5) Du, Y.; Sheng, H.; Astruc, D.; Zhu, M. Atomically Precise Noble Metal Nanoclusters as Efficient Catalysts: A Bridge between Structure and Properties. *Chem. Rev.* **2020,** *120*, 526-622, DOI: 10.1021/acs.chemrev.8b00726.

(6) Yamazoe, S.; Koyasu, K.; Tsukuda, T. Nonscalable Oxidation Catalysis of Gold Clusters. *Acc. Chem. Res.* **2014,** *47*, 816-824, DOI: 10.1021/ar400209a.

(7) Chakraborty, I.; Pradeep, T. Atomically Precise Clusters of Noble Metals: Emerging Link between Atoms and Nanoparticles. *Chem. Rev.* **2017,** *117*, 8208-8271, DOI: 10.1021/acs.chemrev.6b00769.

(8) Konishi, K. Phosphine-Coordinated Pure-Gold Clusters: Diverse Geometrical Structures and Unique Optical Properties/Responses. *Struct. Bond.* **2014,** *161*, 49-86, DOI: 10.1007/430_2014_143.

(9) Konishi, K.; Iwasaki, M.; Sugiuchi, M.; Shichibu, Y. Ligand-Based Toolboxes for Tuning of the Optical Properties of Subnanometer Gold Clusters. *J. Phys. Chem. Lett.* **2016,** *7*, 4267-4274, DOI: 10.1021/acs.jpclett.6b01999.

(10) Mingos, D. M. P. Structural and Bonding Patterns in Gold Clusters. *Dalton Trans.* **2015,** *44*, 6680-6695, DOI: 10.1039/C5DT00253B.

(11) Zhou, M.; Higaki, T.; Hu, G.; Sfeir, M. Y.; Chen, Y.; Jiang, D.; Jin, R. Three-Orders-of-Magnitude Variation of Carrier Lifetimes with Crystal Phase of Gold Nanoclusters. *Science* **2019,** *364*, 279-282, DOI: 10.1126/science.aaw8007.

(12) Iwasaki, M.; Kobayashi, N.; Shichibu, Y.; Konishi, K. Facile Modulation of Optical Properties of Octagold Clusters through the Control of Ligand-Mediated Interactions. *Phys. Chem. Chem. Phys.* **2016,** *18*, 19433-19439, DOI: 10.1039/C6CP03129C.

(13) Iwasaki, M.; Shichibu, Y.; Konishi, K. Unusual Attractive Au-π Interactions in Small Diacetylene-Modified Gold Clusters. *Angew. Chem. Int. Ed.* **2019,** *58*, 2443-2447, DOI: 10.1002/anie.201814359.

(14) Bakar, M. A.; Sugiuchi, M.; Iwasaki, M.; Shichibu, Y.; Konishi, K. Hydrogen bonds to Au atoms in coordinated gold clusters. *Nature Commun.* **2017,** *8*, 576, DOI: 10.1038/s41467-017-00720-3.

(15) Nieto-Ortega, B.; Bürgi, T. Vibrational Properties of Thiolate-Protected Gold Nanoclusters. *Acc. Chem. Res.* **2018,** *51,* 2811-2819, DOI: 10.1021/acs.accounts.8b00376.

(16) Aikens, C. M. Electronic and Geometric Structure, Optical Properties, and Excited State Behavior in Atomically Precise Thiolate-Stabilized Noble Metal Nanoclusters. *Acc. Chem. Res.* **2018,** *51,* 3065-3073, DOI: 10.1021/acs.accounts.8b00364.

(17) Yasuda, S.; Tamura, K.; Terasawa, T.-o.; Yano, M.; Nakajima, H.; Morimoto, T.; Okazaki, T.; Agari, R.; Takahashi, Y.; Kato, M.; Yagi, I.; Asaoka, H. Confinement of Hydrogen Molecules at Graphene–Metal Interface by Electrochemical Hydrogen Evolution Reaction. *J. Phys. Chem. C* **2020,** *124*, 5300-5307, DOI: 10.1021/acs.jpcc.0c00995.

(18) Frank, O.; Vejpravova, J.; Holy, V.; Kavan, L.; Kalbac, M. Interaction between Graphene and Copper Substrate: The Role of Lattice Orientation. *Carbon* **2014,** *68*, 440-451, DOI: https://doi.org/10.1016/j.carbon.2013.11.020.

(19) Huang, M.; Yan, H.; Chen, C.; Song, D.; Heinz, T. F.; Hone, J. Phonon Softening and Crystallographic Orientation of Strained Graphene Studied by Raman Spectroscopy. *Proc. Natl. Acad. Sci.* **2009,** *106*, 7304-7308, DOI: 10.1073/pnas.0811754106.

(20) Senanayake, R. D.; Akimov, A. V.; Aikens, C. M. Theoretical Investigation of Electron and Nuclear Dynamics in the $[Au_{25}(SH)_{18}]^{-1}$ Thiolate-Protected Gold Nanocluster. *J. Phys. Chem. C* **2017,** *121*, 10653-10662, DOI: 10.1021/acs.jpcc.6b09731.

(21) Senanayake, R. D.; Guidez, E. B.; Neukirch, A. J.; Prezhdo, O. V.; Aikens, C. M. Theoretical Investigation of Relaxation Dynamics in $Au_{38}(SH)_{24}$ Thiolate-Protected Gold Nanoclusters. *J. Phys. Chem. C* **2018,** *122*, 16380-16388, DOI: 10.1021/acs.jpcc.8b03595.

(22) Palacios-Álvarez, O.; Tlahuice-Flores, A. Tri-Icosahedral $Au_{37}$ Cluster as a Carrier/Detector for Anti-Cancer Cisplatin Drug. *J. Raman Spectrosc.* **2019,** *50*, 52-62, DOI: 10.1002/jrs.5498.

(23) Varnholt, B.; Guberman-Pfeffer, M. J.; Oulevey, P.; Antonello, S.; Dainese, T.; Gascón, J. A.; Bürgi, T.; Maran, F. Vibrational Coupling Modulation in n-Alkanethiolate Protected $Au_{25}(SR)_{180}$ Clusters. *J. Phys. Chem. C* **2016,** *120*, 25378-25386, DOI: 10.1021/acs.jpcc.6b07592.

(24) Zhou, M.; Tian, S.; Zeng, C.; Sfeir, M. Y.; Wu, Z.; Jin, R. Ultrafast Relaxation Dynamics of $Au_{38}(SC_2H_4Ph)_{24}$ Nanoclusters and Effects of Structural Isomerism. *J. Phys. Chem. C* **2017,** *121*, 10686-10693, DOI: 10.1021/acs.jpcc.6b10360.

(25) Sfeir, M. Y.; Qian, H.; Nobusada, K.; Jin, R. Ultrafast Relaxation Dynamics of Rod-Shaped 25-Atom Gold Nanoclusters. *J. Phys. Chem. C* **2011,** *115*, 6200-6207, DOI: 10.1021/jp110703e.

(26) Maioli, P.; Stoll, T.; Sauceda, H. E.; Valencia, I.; Demessence, A.; Bertorelle, F.; Crut, A.; Vallée, F.; Garzón, I. L.; Cerullo, G.; Del Fatti, N. Mechanical Vibrations of Atomically Defined Metal Clusters: From Nano- to Molecular-Size Oscillators. *Nano Lett.* **2018,** *18*, 6842-6849, DOI: 10.1021/acs.nanolett.8b02717.

(27) Portales, H.; Goubet, N.; Saviot, L.; Adichtchev, S.; Murray, D. B.; Mermet, A.; Duval, E.; Pileni, M. P. Probing Atomic Ordering and Multiple Twinning in Metal Nanocrystals through Their Vibrations. *Proc. Natl. Acad. Sci. USA* **2008,** *105*, 14784-14789, DOI: 10.1073/pnas.0803748105.

(28) Portales, H.; Saviot, L.; Duval, E.; Fujii, M.; Hayashi, S.; Fatti, N. D.; Vallée, F. Resonant Raman Scattering by Breathing Modes of Metal Nanoparticles. *J. Chem. Phys.* **2001,** *115*, 3444-3447, DOI: 10.1063/1.1396817.

(29) Sinha, K.; Menéndez, J. First- and Second-Order Resonant Raman Scattering in Graphite. *Phys. Rev. B* **1990,** *41*, 10845-10847, DOI: 10.1103/PhysRevB.41.10845.

(30) Tan, P. H.; Han, W. P.; Zhao, W. J.; Wu, Z. H.; Chang, K.; Wang, H.; Wang, Y. F.; Bonini, N.; Marzari, N.; Pugno, N.; Savini, G.; Lombardo, A.; Ferrari, A. C. The Shear Mode of Multilayer Graphene. *Nature Mater.* **2012,** *11*, 294-300, DOI: 10.1038/nmat3245.

(31) Glebov, A.; Mokhun, O.; Rapaport, A.; Vergnole, S.; Smirnov, V.; Glebov, L. *Volume Bragg Gratings as Ultra-Narrow and Multiband Optical Filters*. Proc. SPIE: 2012; Vol. 8428, p 84280C, DOI: 10.1117/12.923575.

(32) Inagaki, M.; Motobayashi, K.; Ikeda, K. Electrochemical THz-SERS Observation of Thiol Monolayers on Au(111) and (100) Using Nanoparticle-assisted Gap-Mode Plasmon Excitation. *J. Phys. Chem. Lett.* **2017,** *8*, 4236-4240, DOI: 10.1021/acs.jpclett.7b01901.

(33) Kamei, Y.; Shichibu, Y.; Konishi, K. Generation of Small Gold Clusters with Unique Geometries through Cluster-to-Cluster Transformations: Octanuclear Clusters with Edge-sharing Gold Tetrahedron Motifs. *Angew. Chem. Int. Ed.* **2011,** *50*, 7442-7445, DOI: 10.1002/anie.201102901.

(34) Gutrath, B. S.; Schiefer, F.; Homberger, M.; Englert, U.; Şerb, M.-D.; Bettray, W.; Beljakov, I.; Meded, V.; Wenzel, W.; Simon, U. Molecular and Electronic Structure of the

Cluster $[Au_8(PPh_3)_8](NO_3)_2$. *Eur. J. Inorg. Chem.* **2016,** *2016,* 975-981, DOI: 10.1002/ejic.201501334.

(35) Van der Velden, J. W. A.; Bour, J. J.; Bosman, W. P.; Noordik, J. H. Reactions of cationic gold clusters with Lewis bases. Preparation and X-ray structure investigation of $[Au_8(PPh_3)_7](NO_3)_2 \cdot 2CH_2Cl_2$ and $Au_6(PPh_3)_4[Co(CO)_4]_2$. *Inorg. Chem.* **1983,** *22,* 1913-1918, DOI: 10.1021/ic00155a018.

(36) Kobayashi, N.; Kamei, Y.; Shichibu, Y.; Konishi, K. Protonation-Induced Chromism of Pyridylethynyl-Appended [core+exo]-Type $Au_8$ Clusters. Resonance-Coupled Electronic Perturbation through $\pi$-Conjugated Group. *J. Am. Chem. Soc.* **2013,** *135,* 16078-16081, DOI: 10.1021/ja4099092.